energy&fuels

Article

Cite This: Energy Fuels 2019, 33, 3421−3428

pubs.acs.org/EF

Effect of Ionic Liquid Impregnation in Highly Water-Stable Metal−Organic Frameworks, Covalent Organic Frameworks, and Carbon-Based Adsorbents for Post-combustion Flue Gas Treatment

Manish Maurya and Jayant K. Singh*

Department of Chemical Engineering, Indian Institute of Technology Kanpur, Kanpur, Uttar Pradesh 208016, India

ABSTRACT: In this work, a comparative study on water-stable microporous adsorbents is conducted computationally in the quest of a suitable adsorbent for post-combustion CO_2 capture. In this regard, three metal−organic frameworks (MOFs), two covalent organic frameworks (COFs), and a single-wall carbon nanotube (SWCNT) are investigated under the same flue gas conditions. The simulation results show that the pure component adsorption capacity for CO_2 follows the order SWCNT > InOF-1 > COF-300 > UiO-66 > COF-108 > ZIF-8 at post-combustion conditions. Further, these materials are impregnated with ionic liquids to examine the effect on the CO_2 separation ability of these materials. The adsorption capacity enhances by incorporating ionic liquids, especially [EMIM][SCN] compared to [EMIM][BF_4] as a result of a stronger interaction and being less bulky in nature. We further tested the effect of the presence of other components of flue gas on the selectivity of CO_2 over N_2, and we found that the presence of SO_2 and water vapor reduces the CO_2 selectivity in all of the materials considered in this work. Performance in terms of CO_2 selectivity of these materials is tested in the presence of all major components of flue gas, and we found that, under the same thermodynamic conditions, it follows the order InOF-1 > COF-300 > UiO-66 > SWCNT > COF-108 ≈ ZIF-8. The CO_2/N_2 selectivity increases significantly after impregnating materials with ionic liquids. In the presence of water, InOF-1 completely discard N_2, showing infinitely large selectivity for CO_2/N_2. In humid conditions, the difference in selectivity between pristine and composite materials decreases significantly.

INTRODUCTION

Global warming caused by the emission of greenhouse gases from different sources, such as thermoelectric power plants and industrial plants, is one of the biggest threats to our environment. CO_2, the principal greenhouse gas, is responsible for global warming and climate change. The average annual growth rate of the CO_2 concentration in the environment has increased from 1 ppm/year in the 1970s to more than 2 ppm/year in the current decade. As a result of this, the CO_2 concentration in the atmosphere has crossed the level of 400 ppm.[1] It is expected that, with the stable rate of emission in a few decades, the CO_2 concentration will reach 550 ppm in 2050. The human body will start suffering once the CO_2 concentration crosses the 600 ppm limit.[2] According to the report published in 2017 by the International Energy Agency, currently, the power plant industry alone is responsible for 41% of the global CO_2 emissions, followed by transportation (23%), petrochemical industries (20%), building sector (10%), and others. While more research is required to effectively use renewable energy resources on a large-scale energy requirement, non-renewable energy resources (fossil fuels) will remain the primary source of energy for power plant industries and transportation for many years to come. Therefore, controlling the emissions from major point sources has become increasingly urgent.

In this context, the technology of carbon capture and storage (CCS) has received overwhelming attention over the past few decades as a potential method of mitigating CO_2. Among the different techniques available for CO_2 separation, gas absorption using aqueous amine solution has been used for decades to capture CO_2 on an industrial scale.[3−8] However, such amine scrubbing has serious drawbacks, such as the loss of solvent, corrosion of equipment, and high-energy demand for regeneration of the absorbent, as a result of the strong binding with CO_2. Different approaches are being used to cope with this drawback of amine-based CO_2 separation technology. Recently, Bernard et al. have examined that the mixture of amine and ionic liquids (ILs) has potential to reduce the energy requirement in the desorption process. It also helps in tuning viscosity and vapor pressure of amine solvents, resulting in the reduction of the loss of solvents. Apart from this, polymerized ILs are also being investigated to enhance CO_2 adsorption.[9,10] Another approach to separate CO_2 from flue gas stream is through the use of membranes. Several types of membrane materials, such as polymeric membranes, inorganic membranes, and mixed matrix membranes, have been used for CO_2 capture.[11−13] Developing new membranes with both high permeability and selectivity can be significantly more efficient for CO_2 separation than liquid absorption processes. Brunetti et al.[14] pointed out that the performance of a membrane system is strongly affected by the flue gas conditions, such as a low CO_2 concentration and pressure, which are the main hurdles for applying this technology. According to Bernardo et al.,[15] although there are significant developments in gas separation membrane systems, they are still far away to realize the potentialities of this technology as a result of low fluxes and selectivity issues.

Received: January 18, 2019
Revised: March 13, 2019
Published: March 15, 2019

DOI: 10.1021/acs.energyfuels.9b00179
Energy Fuels 2019, 33, 3421−3428

Hence, the development of alternative technologies for carbon capture based on porous adsorbents is being pursued because the process is clean and has smaller energy requirements during the regeneration cycle. In this regard, several porous materials have been investigated for CO_2 capture, such as zeolites,[16,17] carbon-based adsorbents,[18−22] metal−organic frameworks (MOFs),[23−26] and covalent organic frameworks (COFs).[27−30] For practical applicability of adsorbents at industrial scale, the particular requirements are high CO_2 selectivity in the mixture of flue gases, high adsorption capacity at post-combustion conditions, and structural stability under humid conditions. Most of the best performing adsorbents are not stable under humid conditions because the typical composition of coal-fired flue gas is as follows: 73−77% N_2, 15−16% CO_2, 5−7% H_2O, 3−4% O_2, 800 ppm of SO_2, and traces of other impurities.[31] It is challenging to compare the adsorption performance of different adsorbents in the literature and draw universal conclusions about the practical applicability of adsorbents at post-combustion conditions as a result of the variable condition and assumption made in the literature. We want to maintain the same condition while comparing different adsorbents. These conditions are temperature, pressure, and most importantly real gas compositions. In most of the studies, authors have taken different compositions of different gas mixtures at different temperature and pressure conditions, which makes things difficult to compare.

Therefore, with this motivation, a computational study is conducted to compare the performance of highly water-stable MOFs,[32−34] COFs, and carbon-based adsorbents for the practical applicability in CCS. We have further compared their performance by impregnating with different room-temperature ILs to enhance the selectivity. It is envisaged that this study will provide a better understanding of materials that have the potential to be used at post-combustion conditions in CCS.

MODELS AND COMPUTATIONAL METHODS

Structures and Force Fields of Different Adsorbents and ILs. In this study, as representatives of water-stable adsorbents, we have selected six different adsorbents that consist of three MOFs, viz., InOF-1, ZIF-8, UiO-66, and three carbon-based adsorbents, such as COF-108, COF-300, and hexagonally arranged single-wall carbon nanotube (SWCNT).[33−35] All of the framework structures are taken from crystallographic data reported in the literature. The information on the unit cell of each material is given in Table 3. To improve the separation efficiency of these materials, we have considered imidazolium-based ILs to impregnate these materials because the use of bulk ILs at the industrial scale is problematic because of their high viscosity and need for a high quantity and low rate of mass transport. It is also a fact that room-temperature ILs are very expansive compared to the amine-based ILs, and hence, cost effectiveness of the process involving bulk room-temperature ILs for CO_2 separation is not comparable to an alternative adsorptive technique. An average cost of room-temperature IL on the basis of per unit mass is about 100−1000 times more than the conventional amine-based ILs.[36] It is reported in the literature that the type of anions completely determines the selectivity of ILs for CO_2, while the type of cations has a negligible effect.[37] Therefore, we have considered the most favorable anions as $[BF_4]^-$ and $[SCN]^-$, along with $[EMIM]^+$, for CO_2 separation.[38,39] The optimized molecular models of IL pairs are shown in Figure 1. The interaction potential parameters for MOFs and COFs are taken from the universal force field (UFF) and DREIDING force field that are listed in Tables 1 and 2, respectively.[40−44] The density functional theory (DFT) is used to calculate the partial charges of InOF-1 and geometry optimization of the pair of ILs using the Gaussian 09 package. Partial charges are calculated using Mulliken population analysis with the split basis set and Becke, three-parameter, Lee−Yang−Parr (B3LYP) hybrid functional. The LANL2DZ basis set is used for the In atom, whereas 6-31G is used for rest of the atoms. The partial charges of MOFs other than InOF-1 and partial charges of COFs are taken from the UFF and DREIDING force field. The potential parameters for SWCNT are taken from the AMBER96 force field.[45] We have not compared the results to different force fields; we stick to the force fields that are used in the literature for such studies. MOF and COF structures are mostly modeled using UFF and DREIDING force field for adsorption studies. The carbon nanotube is modeled by AMBER force fields for the CO_2 adsorption study in the literature. The radius, the length of the SWCNT, and the intertube distance used in this work are 1.5, 5, and 1 nm, respectively. The force field parameters of $[EMIM]^+$ are taken from Manish et al.;[46] the force field parameters of

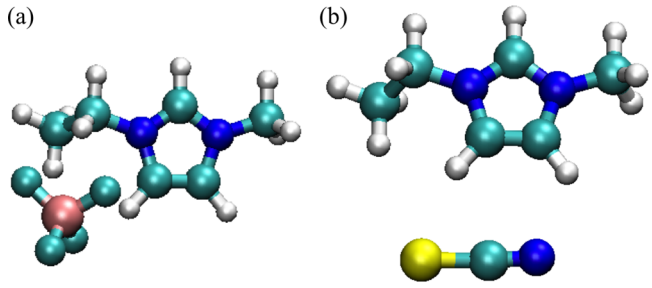

Figure 1. Optimized molecular model of (a) $[EMIM][BF_4]$ and (b) [EMIM][SCN] used in simulations. The color coding is as follows: carbon (cyan), nitrogen (blue), boron (pink), sulfur (yellow), and hydrogen (white).

Table 1. Force Field Parameters of MOFs Considered in This Work

molecule	site	ε (K)	σ (Å)	q (e)
InOF-1	C1	47.856	3.473	0.0576
	C2	47.856	3.473	−0.1084
	C3	47.856	3.473	0.0756
	C4	47.856	3.473	−0.0623
	C5	47.856	3.473	0.5244
	H1	7.649	2.847	0.0926
	H2	7.649	2.847	0.1398
	H3	0.0	2.571	0.3978
	O1	7.649	2.847	0.0926
	O2	7.649	2.847	0.0926
	O3	7.649	2.847	0.0926
	In	0.0	3.976	1.6634
UiO-66	C1	46.421	3.369	0.625
	C2	46.421	3.369	−0.002
	C3	46.421	3.369	−0.121
	H1	7.419	2.761	0.127
	H2	7.419	2.761	0.495
	O1	46.713	2.942	−0.582
	O2	46.713	2.942	−1.179
	O3	46.713	2.942	−0.741
	Zr	33.68	2.70	2.008
ZIF-8	C1	33.565	3.431	0.429
	C2	33.565	3.431	−0.08485
	C3	33.565	3.431	−0.4526
	H1	14.04	2.571	0.1128
	H2	14.04	2.571	0.1325
	Zn	39.604	2.462	0.6918
	N	22.0412	3.261	−0.388

DOI: 10.1021/acs.energyfuels.9b00179
Energy Fuels 2019, 33, 3421−3428

Table 2. Force Field Parameters of COFs and SWCNT Considered in This Work

molecule	site	ε (K)	σ (Å)	q (e)
COF-108	C1	47.86	3.47	0.260
	C2	47.86	3.47	−0.332
	C3	47.86	3.47	0.045
	C4	47.86	3.47	−0.165
	C5	47.86	3.47	−0.104
	C6	47.86	3.47	−0.154
	C7	47.86	3.47	0.156
	C8	47.86	3.47	0.076
	H1	7.650	2.85	0.190
	H2	7.650	2.85	0.110
	H3	7.650	2.85	0.093
	O1	48.16	3.03	−0.418
	B1	47.81	3.58	0.610
COF-300	C1	47.86	3.47	0.024
	C2	47.86	3.47	−0.023
	C3	47.86	3.47	0.024
	C4	47.86	3.47	0.193
	C5	47.86	3.47	−0.161
	C6	47.86	3.47	0.453
	C7	47.86	3.47	−0.341
	C8	47.86	3.47	−0.090
	C9	47.86	3.47	0.069
	C10	47.86	3.47	−0.341
	H1	7.650	2.85	0.075
	H2	7.650	2.85	0.028
	H3	7.650	2.85	0.130
	H4	7.650	2.85	0.169
	H5	7.650	2.85	0.105
	H6	7.650	2.85	0.169
	N	38.95	3.26	−0.480
SWCNT	C	43.298	3.4	0.0

Table 3. Number of ILs and Unit Cells Used in the Simulation

adsorbent	number of unit cells	dimensions	number of IL pairs
SWCNT	1 × 1 × 1	a = 38.12, b = 66.16, and c = 51.58	12
COF-108	2 × 2 × 2	a = 28.4, b = 28.4, and c = 28.4	17
COF-300	1 × 1 × 3	a = 28.13, b = 28.13, and c = 8.88	2
InOF-1	2 × 2 × 2	a = 15.57, b = 15.57, and c = 12.32	2
ZIF-8	2 × 2 × 2	a = 16.99, b = 16.99, and c = 16.99	2
UiO-66	2 × 2 × 2	a = 20.98, b = 20.98, and c = 20.98	4

BF_4^- are taken from Lopes et al.;[47] and the force field parameters of $[SCN]^-$ are taken from Chaumont et al.[48]

Potential Model and Simulation Details. Porous structures are impregnated with ILs randomly using Monte Carlo (MC) simulation. The number of impregnated IL molecules are decided on the basis of the free pore volume available in that framework. One pair of IL is used per 10 000 Å^3 of free volume available in that framework. This concentration is further doubled to examine the effect of the IL concentration on the adsorption amount. The term pair of IL in this paper refers to the combination of cation and anion, and it should not be confused with the pair of two different ILs. The free pore volume in the framework is calculated by the helium adsorption method. It is then further equilibrated using molecular dynamics (MD) simulations in the *NVT* ensemble. The MD simulations are run for 2 ns using the LAMMPS package to equilibrate the composite system at room temperature with a time step of 1 fs.[49] While the ILs are being relaxed in the system, the framework atoms are kept frozen. This equilibrated structure is further used for adsorption analysis. Grand canonical Monte Carlo (GCMC) simulations are performed to investigate the adsorption capacity of different adsorbents for flue gas using RASPA software.[50] During the MC simulations, composite structures are kept frozen. GCMC simulations are performed at 303 K and pressure up to 2.5 bar. The interaction of adsorbate−adsorbent and adsorbate−adsorbate are modeled as the sum of 12-6 Lennard−Jones (LJ) potential and electrostatic potentials as expressed below

$$E = \sum_{ij} 4\varepsilon_{ij}\left[\left(\frac{\sigma_{ij}}{r_{ij}}\right)^{12} - \left(\frac{\sigma_{ij}}{r_{ij}}\right)^{6}\right] + \sum_{ij}\frac{Cq_iq_j}{r_{ij}} \quad (1)$$

where σ_{ij} and ε_{ij} are collision and well depth parameters between two sites of atoms in the LJ potential model. The interaction energy parameters between unlike atoms are approximated using Lorentz−Berthelot rules [i.e., $\varepsilon_{ij} = (\varepsilon_{ii}\varepsilon_{jj})^{1/2}$ and $\sigma_{ij} = (\sigma_{ii} + \sigma_{jj})/2$].[51] The cutoff distance for dispersion interactions is set at 14 Å, and the long-range electrostatic interactions are calculated using the Ewald sum method. Each MC run consists of 50 000 equilibration and production cycles, where a cycle consists of max(20, N) move attempts (with N being the current number of adsorbed molecules). To visit the important regions of configurational phase space, we have attempted MC moves, such as translation, rotation, and addition/deletion, with probabilities of 0.3, 0.1, and 0.6, respectively. The flue gas during GCMC simulations is first considered as a pure component, and then to study the effect of the presence of other components, it is considered as a mixture of three to five components comprising CO_2, SO_2, O_2, N_2, and H_2O. The TraPPE potential model is used for CO_2, SO_2, O_2, and N_2, and the SPC/E potential is used for H_2O molecules.[52,53] Partial pressures of each species are taken according to the real composition of each component in the flue gas stream. The corresponding mole fractions are 0.16 for CO_2, 0.04 for O_2, 0.316 for H_2O, and 0.008 for SO_2, and the rest is used for N_2 according to the number of components present in the mixture.[31] The absolute adsorption capacity is converted to excess adsorption capacity to compare to experimental results as follows:

$$N_{excess} = N_{ad} - \rho_b V_{free} \quad (2)$$

where ρ_b is the bulk density of gas, which is obtained from independent GCMC simulation at the same thermodynamic conditions, and V_{free} is the free pore volume for the gas molecules. Heat of adsorption is the indication of strength of adsorption of fluid molecules, which is calculated as

$$q_{st} \approx RT - \left(\frac{\partial U_{ad}}{\partial N_{ad}}\right)_{T,V} \quad (3)$$

where U_{ad} is the total energy of the adsorbed phase. During the adsorption of the mixture of flue gases in the porous materials, selectivity of material is a very important parameter to examine the utility of that material commercially. Adsorption selectivity of the surface for species i over species j in a mixture of flue gases is defined as

$$S_{i/j} = \left(\frac{x_i}{x_j}\right)\left(\frac{y_j}{y_i}\right) \quad (4)$$

where x and y are the mole fractions of species in adsorbed and bulk phases, respectively.

RESULTS AND DISCUSSION

Sorption Analysis of Pure Component Flue Gases in Highly Water-Stable MOFs, COFs, and Carbon-Based Adsorbents. Figure 2 shows the pure gas adsorption

DOI: 10.1021/acs.energyfuels.9b00179
Energy Fuels 2019, 33, 3421−3428

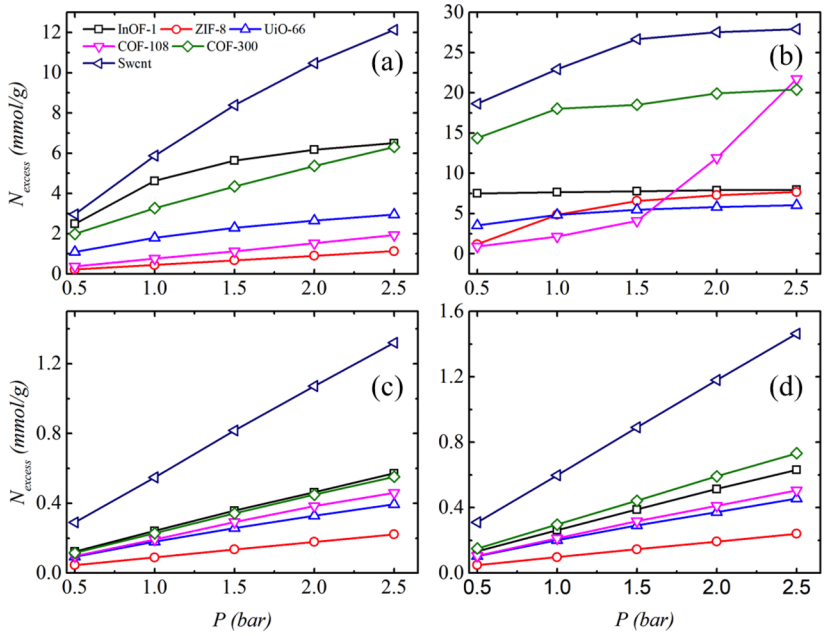

Figure 2. Pure component adsorption isotherms of (a) CO_2, (b) SO_2, (c) N_2, and (d) O_2 in different adsorbents at 303 K.

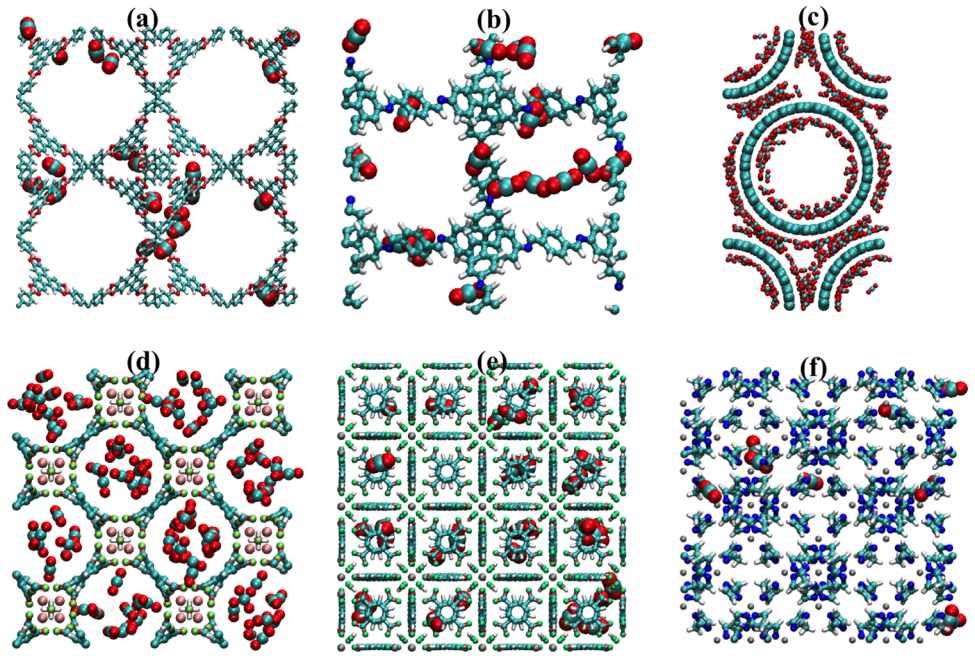

Figure 3. Adsorption of CO_2 in (a) COF-108, (b) COF-300, (c) SWCNT, (d) InOF-1, (e) UiO-66, and (f) ZIF-8 at 1 bar and 303 K. The thick linear molecule containing two red atoms and one cyan atom represents the adsorbed CO_2 molecule.

isotherms of CO_2, SO_2, N_2, and O_2 in InOF-1, ZIF-8, UiO-66, COF-108, COF-300, and SWCNT at 303 K and up to 2.5 bar. These simulation results show the comparative study of the CO_2 capture ability of different highly water-stable adsorbents. It can be seen that CO_2 is more strongly adsorbed in the SWCNT compared to other adsorbents considered in this work. The adsorption capacity of different adsorbents for CO_2 follows the order SWCNT > InOF-1 > COF-300 > UiO-66 > COF-108 and ZIF-8. It is notable from Figure 2b that the SO_2 adsorption capacity is significantly higher than that of CO_2 in each of the adsorbents. This has been reported in previous studies that the uptake of SO_2 is found to be larger than CO_2 in any type of adsorbent whether in carbon-based adsorbents or MOFs.[22,54] This can be attributed to its high dipole moment (1.60 D)[55] and electrostatic interaction compared to CO_2, which has no dipole moment. Although CO_2 has a strong quadrupole moment compared to N_2. The order of the SO_2 adsorption capacity is completely different from CO_2 adsorption; as a result of this, the selectivity of adsorbents during adsorption of a mixture will become affected. Thus, on the basis of pure component adsorption data, we cannot select the best adsorbent for the practical deployment in CCS. We must examine its selectivity for the flue gas components that we want to separate.

The adsorption amounts of N_2 and O_2 as shown in panels c and d of Figure 2 are quite low as a result of the weak

DOI: 10.1021/acs.energyfuels.9b00179
Energy Fuels 2019, 33, 3421−3428

interaction with different adsorbents, although its capacity in the SWCNT is comparatively higher than that in MOFs and COFs. A snapshot of CO_2 adsorption is shown in Figure 3, which reveals the adsorption capacity of different materials under post-combustion conditions. This shows that the materials with wide open pores exhibit less adsorption at a low pressure. Figure 4 shows the heat of adsorption of CO_2 in

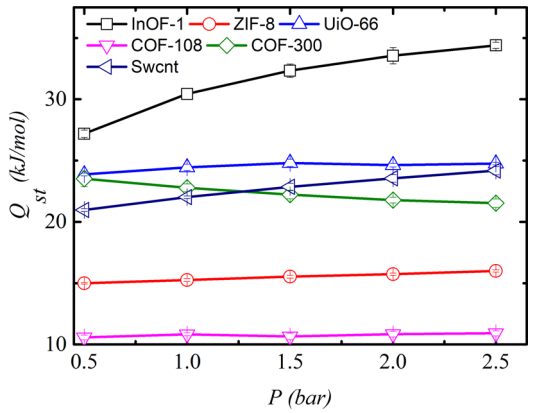

Figure 4. Heat of adsorption of CO_2 in different adsorbents at 303 K.

different adsorbents. The heat of adsorption shows the strength of adsorption with the surface. The magnitude of the heat of adsorption data of CO_2 in different frameworks is as InOF-1 > UiO-66 > COF-300 > SWCNT > ZIF-8 > COF-108. There is a crossover in heat of adsorption data for SWCNT and COF-300 around 1 bar. The total heat of adsorption is the sum of fluid−fluid and fluid−solid interactions. In the case of the SWCNT, contribution from a fluid−fluid interaction increases as a result of the formation of a multilayer of CO_2, as shown in Figure 3c, which enhances the total heat of adsorption, unlike COF-300. The CO_2 uptake capacity and heat of adsorption data are not in the same order. It is evident from the results that the adsorption amount is dictated by not only the strength of adsorption but also the accessible pore volume of that framework. Therefore, merely on the basis of the heat of adsorption data, we cannot screen the material for CO_2 separation. In fact, it is essential to have a large uptake capacity with a low heat of adsorption for adsorptive treatment of the flue gas because it will require less energy during regeneration of the adsorbent. Hence, the uptake capacity and selectivity are the key factors to determine the adsorbent usefulness in CCS technology.

Effect of ILs on the Sorption Capacity of Adsorbents. After comparing the adsorption capacity of different water-stable materials for flue gas stream, we focus on how the composites of these materials with IL will perform in gas separation technology. Therefore, in this regard, the adsorption capacity of composite materials for CO_2 is tested, and results are shown in Figure 5. These results indicate that the composites of IL with solid adsorbents do not enhance the uptake capacity of all types of solid frameworks. As in the case of InOF-1, the effect of IL impregnation has a negative effect on gas uptake, whereas impregnation of ILs in other porous materials enhances the CO_2 uptake capacity. This is due to less accessible volume available in the narrow pore size of InOF-1. The SWCNT also shows negligible improvement in adsorption capacity upon being impregnated with ILs. The pore size distribution in all of these materials is shown in Figure 6. It

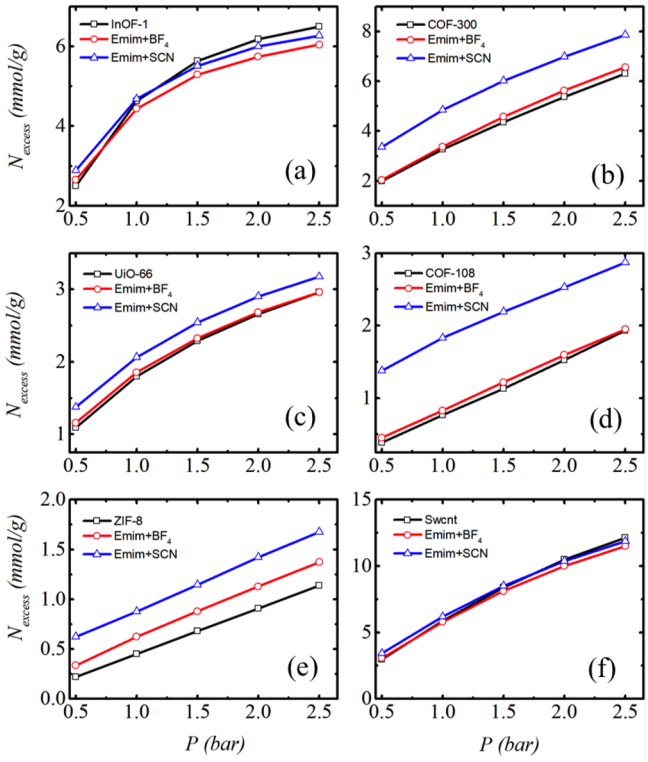

Figure 5. Adsorption isotherms of CO_2 in pristine and IL-impregnated adsorbents, such as (a) InOF-1, (b) COF-300, (c) UiO-66, (d) COF-108, (e) ZIF-8, and (f) SWCNT, at 303 K.

shows that the InOF-1 framework has the smallest pores, followed by UiO and COF frameworks.

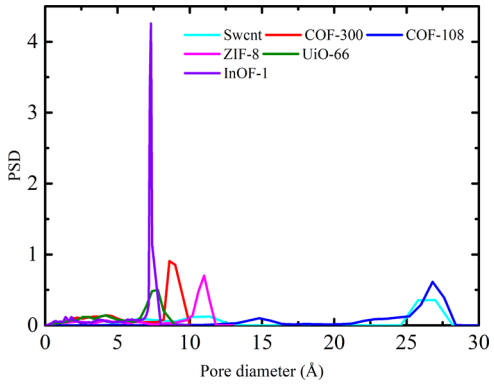

Figure 6. Pore size distribution in different frameworks under consideration.

The increment in uptake capacity of CO_2 is more in the case of the [EMIM][SCN] pair compared to [EMIM][BF_4] in all of the porous materials. This is because the binding of CO_2 with $[SCN]^-$ is more compared to $[BF_4]^-$, as supported by the DFT calculations. As described by Gupta et al., the binding strength of CO_2 with different ILs follows the order $[PF_6]^- < [Tf_2N]^- < [BF_4]^- < [SCN]^-$.[56] In the case of InOF-1, shown in Figure 5a, the available pore space decreases significantly, as a result of which the capacity decreases with respect to the pristine structure. Impregnating porous materials with ILs improves the performance for gas separation, but this enhancement is not adequate in comparison to the adsorption capacity of the SWCNT. Pure COF-300 has CO_2 uptake of 3

DOI: 10.1021/acs.energyfuels.9b00179
Energy Fuels 2019, 33, 3421−3428

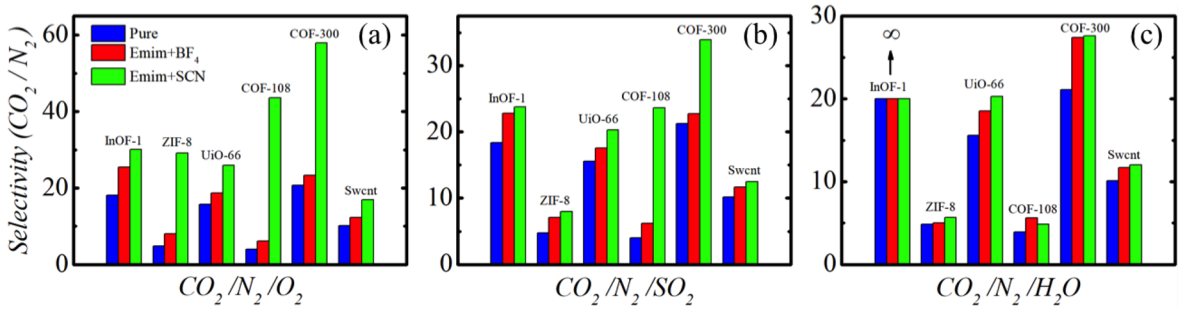

Figure 7. Selectivity of CO_2 over N_2 in the ternary mixture of (a) $CO_2/N_2/O_2$, (b) $CO_2/N_2/SO_2$, and (c) $CO_2/N_2/H_2O$.

mmol/g at 1 bar. The composite of COF-300 and [EMIM]-[SCN] enhances the adsorption capacity for CO_2 to 5 mmol/g at 1 bar, as shown in Figure 5b. It is observed that the effect of $[BF_4]^-$ is very small compared to $[SCN]^-$, which can also be seen in the case of UiO-66 (Figure 5c), COF-108 (Figure 5d), ZIF-8 (Figure 5e), and SWCNT (Figure 5f). We have found that, after increasing the IL concentration by 2 times in porous structures, the adsorption capacity either further decreases or shows negligible improvements in some materials. Apart from determining the effect of the IL on CO_2 uptake capacity, it would be pertinent to analyze the selective gas separation ability of the considered composite materials.

Selectivity Analysis of Flue Gas Mixtures. In the previous section, we compared the effect of IL impregnation in water-stable MOFs, COFs, and SWCNT to enhance the uptake capacity. Now, we turn our attention to examine the effect of IL impregnation, in the considered adsorbents, on the selective separation of CO_2 from the flue gas. The selectivity for CO_2 over N_2 in any kind of adsorbent is the most important factor for its usage in the gas separation techniques. Therefore, a comparative study of the simulated adsorption selectivity of different adsorbents for CO_2/N_2 is conducted, which is shown in Figure 7. The results indicate that the composite materials enhance the adsorption selectivity for CO_2 compared to pristine materials. This is due to the fact that the binding strength of CO_2 with ILs is more compared to N_2. This binding strength becomes increased with the use of the SCN anion, as shown in DFT calculations.[56] Hence, the selectivity of porous materials impregnated with [EMIM]-[SCN] IL is more compared to [EMIM][BF_4]. Apart from the binding strength, the exposure of strong binding sites of ILs to gas molecules is equally important, and therefore, dispersion of ILs through the porous materials is crucial.

Because the selectivity of adsorbents for CO_2/N_2 is known to become affected in the presence of other flue gas components, three different mixtures are considered, such as $CO_2/N_2/O_2$, $CO_2/N_2/SO_2$, and $CO_2/N_2/H_2O$. Figure 7a shows the selectivity of CO_2 over N_2 in a mixture of $CO_2/N_2/O_2$. These results indicate that the composite materials show enhanced selectivity compared to the pristine framework. The maximum enhancement is observed in COFs, followed by MOFs and carbon-based adsorbents. Among pristine frameworks, COF-300 shows the maximum selectivity for CO_2, followed by InOF-1, UiO-66, SWCNT, and ZIF-8, with the least for COF-108. Although the excess adsorption amount in InOF-1 is decreased, the selectivity for CO_2 has increased after inserting ILs.

The effect of $[SCN]^-$ compared to $[BF_4]^-$ is more on selective separation of CO_2 from N_2 in all adsorbents, which strongly suggests that $[SCN]^-$ is most useful to make composite materials. After including SO_2 in place of O_2 in the mixture, as shown in Figure 7b, the selectivity for CO_2/N_2 decreases in composite materials. The selectivity of pristine materials in the mixture of $CO_2/N_2/SO_2$ does not change much with respect to the selectivity in the mixture of $CO_2/N_2/O_2$. This indicates that SO_2 is preferably adsorbed in composite materials than CO_2. The presence of water vapor (shown in Figure 7c) also reduces the selectivity of composite materials. In moist conditions, InOF-1 rejects nitrogen adsorption completely as a result of the fact that the adsorption of water is significantly high, leading toward very high selectivity of CO_2 over N_2. In humid conditions, the selectivity of COF-108 for CO_2 is significantly suppressed; moreover, the selectivity value of COF-108 composites based on $[BF_4]^-$ shows a higher value than that based on $[SCN]^-$. The difference between selectivity values in pristine and composite materials is suppressed by a large number in humid conditions. In the SWCNT, the effect of water vapor is negligible in both pristine and composite frameworks, although the selectivity is less than that of some MOFs and COFs.

To examine the applicability of these materials in actual conditions, we have calculated selectivity of materials for CO_2 and SO_2 in the mixture of $CO_2/N_2/O_2/SO_2/H_2O$, which is shown in Figure 8. Figure 8a presents the CO_2/N_2 selectivity in the actual flue gas mixture at 1 bar and 303 K. The order of selectivity of different materials is as follows: InOF-1 > COF-300 > UiO-66 > SWCNT > ZIF-8 > COF-108. As a result of the presence of water, InOF-1 shows huge attraction toward water vapor and almost negligible adsorption of N_2, resulting in an infinitely large value of selectivity. The adsorption amount of CO_2 is also less compared to water uptake. These selectivity data comprise the effect of O_2, SO_2, and water vapor on selective adsorption of CO_2.

Figure 8b shows the simulated selectivity of SO_2 over CO_2 in the actual flue gas adsorption. This selectivity is important while separating SO_2 from the mixture of flue gas because the presence of SO_2 adversely affects the separation of CO_2. As one of the reasons for acidic rain, it needs to be eliminated from the flue gas stream, for which the selectivity of the adsorbent toward SO_2 should be high. The order of selectivity obtained in IL-impregnated adsorbents from the simulation is as follows: InOF-1 > UiO-66 > SWCNT > COF-300 > COF-108 > ZIF-8.

The selectivity data of CO_2/N_2 and SO_2/CO_2 are an indicator of the expected selectivity that we can obtain at post-combustion conditions using these MOFs, COFs, and SWCNT. The performance of the composite frameworks is improved significantly over pristine frameworks.

DOI: 10.1021/acs.energyfuels.9b00179
Energy Fuels 2019, 33, 3421−3428

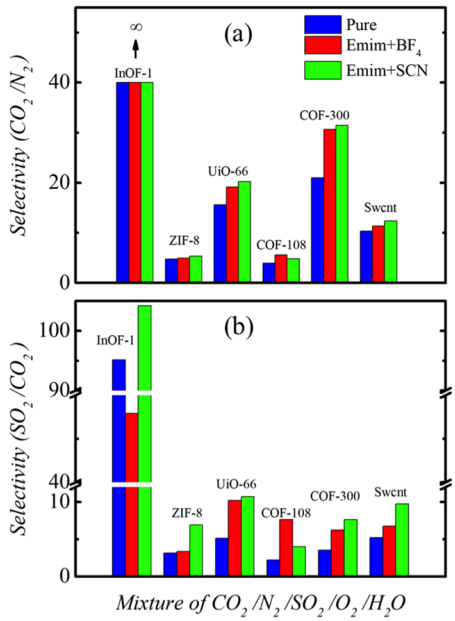

Figure 8. Selectivity of materials for (a) CO_2/N_2 and (b) SO_2/CO_2 when all of the major components of flue gas are present in the flue gas stream.

CONCLUSION

We have selected the best performing water-stable MOFs (InOF-1, UiO-66, and ZIF-8), COFs (COF-108 and COF-300), and carbon-based materials (SWCNT) to investigate the potential material for post-combustion CO_2 capture at power plant industries. For that, we have compared the adsorption capacity and selectivity of these materials under the same thermodynamic conditions using GCMC simulations. The results show that the uptake capacity for CO_2 at post-combustion conditions in these selected adsorbents follows the order SWCNT > InOF-1 > COF-300 > UiO-66 > COF-108 > ZIF-8. We further modified these materials to improve the CO_2 adsorption capacity by impregnating with ILs. The insertion of ILs inside the porous materials enhances the adsorption strength and corresponding adsorption capacity and selectivity of the materials. Further, we assess the effect of the presence of O_2, SO_2, and water vapor on the selectivity of CO_2/N_2 for different materials. Pristine and IL-impregnated COF-300 shows the maximum selectivity for CO_2/N_2 in different ternary mixtures. It is found that the presence of SO_2 and water vapor in the mixture reduces the adsorption selectivity for CO_2/N_2.

Finally, we examined the selectivity of different materials for CO_2/N_2 in an actual flue gas mixture, and it follows the order InOF-1 > COF-300 > UiO-66 > SWCNT > COF-108 ≈ ZIF-8. IL impregnation improves the selectivity of materials by many folds. The IL pair of [EMIM][SCN] is more effective in enhancing the selective separation of CO_2 than the [EMIM]-[BF_4] pair. On the basis of the selectivity analysis of different frameworks under real conditions, the composites of COF-300 and InOF-1 frameworks with ILs are found to be the most useful materials for post-combustion CO_2 capture.

AUTHOR INFORMATION

Corresponding Author

*E-mail: jayantks@iitk.ac.in.

ORCID

Jayant K. Singh: 0000-0001-8056-2115

Notes

The authors declare no competing financial interest.

ACKNOWLEDGMENTS

The authors acknowledge the Ministry of Earth Sciences, Government of India. The authors also acknowledge the high-performance computational facility of the Indian Institute of Technology Kanpur, India.

REFERENCES

(1) Sayari, A.; Belmabkhout, Y.; Serna-Guerrero, R. Flue Gas Treatment via CO_2 Adsorption. *Chem. Eng. J.* **2011**, *171*, 760−774.

(2) Oschatz, M.; Antonietti, M. A Search for Selectivity to Enable CO_2 Capture with Porous Adsorbents. *Energy Environ. Sci.* **2018**, *11*, 57−70.

(3) Luis, P. Use of Monoethanolamine (MEA) for CO_2 Capture in a Global Scenario: Consequences and Alternatives. *Desalination* **2016**, *380*, 93−99.

(4) Dutcher, B.; Fan, M.; Russell, A. G. Amine-Based CO_2 Capture Technology Development from the Beginning of 2013A Review. *ACS Appl. Mater. Interfaces* **2015**, *7*, 2137−2148.

(5) Bhown, A. S.; Freeman, B. C. Analysis and Status of Post-Combustion Carbon Dioxide Capture Technologies. *Environ. Sci. Technol.* **2011**, *45*, 8624−8632.

(6) Knudsen, J. N.; Jensen, J. N.; Vilhelmsen, P.-J.; Biede, O. Experience with CO_2 capture from coal flue gas in pilot-scale: Testing of different amine solvents. *Energy Procedia* **2009**, *1*, 783−790.

(7) Veawab, A.; Aroonwilas, A.; Tontiwachwuthikul, P. CO_2 Absorption Performance of Aqueous Alkanolamines in Packed Columns. *Prepr. Pap.—Am. Chem. Soc., Div. Fuel Chem.* **2002**, *47* (1), 49−50.

(8) Aaron, D.; Tsouris, C. Separation of CO_2 from Flue Gas: A Review. *Sep. Sci. Technol.* **2005**, *40*, 321−348.

(9) Bernard, F. L.; Dalla Vecchia, F.; Rojas, M. F.; Ligabue, R.; Vieira, M. O.; Costa, E. M.; Chaban, V. V.; Einloft, S. Anticorrosion Protection by AmineIonic Liquid Mixtures: Experiments and Simulations. *J. Chem. Eng. Data* **2016**, *61*, 1803−1810.

(10) Bernard, F. L.; Polesso, B. B.; Cobalchini, F. W.; Donato, A. J.; Seferin, M.; Ligabue, R.; Chaban, V. V.; do Nascimento, J. F.; Dalla Vecchia, F.; Einloft, S. CO_2 capture: Tuning cation-anion interaction in urethane based poly(ionic liquids). *Polymer* **2016**, *102*, 199−208.

(11) Prabhakar, R. S.; Freeman, B. D.; Roman, I. Gas and Vapor Sorption and Permeation in Poly(2,2,4-trifluoro-5-trifluoromethoxy-1,3-dioxole-co-tetrafluoroethylene). *Macromolecules* **2004**, *37*, 7688−7697.

(12) Budd, P. M.; Msayib, K. J.; Tattershall, C. E.; Ghanem, B. S.; Reynolds, K. J.; McKeown, N. B.; Fritsch, D. Gas separation membranes from polymers of intrinsic microporosity. *J. Membr. Sci.* **2005**, *251*, 263−269.

(13) Sanders, D. F.; Smith, Z. P.; Guo, R.; Robeson, L. M.; McGrath, J. E.; Paul, D. R.; Freeman, B. D. Energy-efficient polymeric gas separation membranes for a sustainable future: A review. *Polymer* **2013**, *54*, 4729−4761.

(14) Brunetti, A.; Scura, F.; Barbieri, G.; Drioli, E. Membrane Technologies for CO_2 Separation. *J. Membr. Sci.* **2010**, *359*, 115−125.

(15) Bernardo, P.; Drioli, E.; Golemme, G. Membrane Gas Separation: A Review/State of the Art. *Ind. Eng. Chem. Res.* **2009**, *48*, 4638−4663.

(16) Pirngruber, G. D.; Raybaud, P.; Belmabkhout, Y.; Čejka, J.; Zukal, A. The Role of The Extra-Framework Cations in the Adsorption of CO_2 on Faujasite Y. *Phys. Chem. Chem. Phys.* **2010**, *12*, 13534−13546.

(17) Cavenati, S.; Grande, C. A.; Rodrigues, A. E. Adsorption Equilibrium of Methane, Carbon Dioxide, and Nitrogen on Zeolite 13X at High Pressures. *J. Chem. Eng. Data* **2004**, *49*, 1095−1101.

DOI: 10.1021/acs.energyfuels.9b00179
Energy Fuels 2019, 33, 3421−3428

(18) Majumdar, S.; Maurya, M.; Singh, J. K. Adsorptive Separation of CO_2 from Multicomponent Mixtures of Flue Gas in Carbon Nanotube Arrays: A Grand Canonical Monte Carlo Study. *Energy Fuels* **2018**, *32*, 6090−6097.
(19) Na, B.-K.; Koo, K.-K.; Eum, H.-M.; Lee, H.; Song, H. K. CO_2 Recovery from Flue Gas by PSA Process using Activated Carbon. *Korean J. Chem. Eng.* **2001**, *18*, 220−227.
(20) Halder, P.; Maurya, M.; Jain, S. K.; Singh, J. K. Understanding adsorption of CO_2, N_2, CH_4 and their mixtures in functionalized carbon nanopipe arrays. *Phys. Chem. Chem. Phys.* **2016**, *18*, 14007−14016.
(21) Maurya, M.; Singh, J. K. A grand canonical Monte Carlo study of SO_2 capture using functionalized bilayer graphene nanoribbons. *J. Chem. Phys.* **2017**, *146*, 044704.
(22) Maurya, M.; Singh, J. K. Treatment of Flue Gas using Graphene Sponge: A Simulation Study. *J. Phys. Chem. C* **2018**, *122*, 14654−14664.
(23) Grajciar, L.; Wiersum, A. D.; Llewellyn, P. L.; Chang, J.-S.; Nachtigall, P. Understanding CO_2 Adsorption in CuBTC MOF: Comparing Combined DFT ab Initio Calculations with Microcalorimetry Experiments. *J. Phys. Chem. C* **2011**, *115*, 17925−17933.
(24) Simmons, J. M.; Wu, H.; Zhou, W.; Yildirim, T. Carbon Capture in Metal−Organic Frameworks—A Comparative Study. *Energy Environ. Sci.* **2011**, *4*, 2177−2185.
(25) Llewellyn, P. L.; Bourrelly, S.; Serre, C.; Vimont, A.; Daturi, M.; Hamon, L.; De Weireld, G.; Chang, J.-S.; Hong, D.-Y.; Kyu Hwang, Y.; et al. High Uptakes of CO_2 and CH_4 in Mesoporous MetalOrganic Frameworks MIL-100 and MIL-101. *Langmuir* **2008**, *24*, 7245−7250.
(26) Caskey, S. R.; Wong-Foy, A. G.; Matzger, A. J. Dramatic Tuning of Carbon Dioxide Uptake via Metal Substitution in a Coordination Polymer with Cylindrical Pores. *J. Am. Chem. Soc.* **2008**, *130*, 10870−10871.
(27) Zeng, Y.; Zou, R.; Zhao, Y. Covalent Organic Frameworks for CO_2 Capture. *Adv. Mater.* **2016**, *28*, 2855−2873.
(28) Sharma, A.; Malani, A.; Medhekar, N. V.; Babarao, R. CO_2 Adsorption and Separation in Covalent Organic Frameworks with Interlayer Slipping. *CrystEngComm* **2017**, *19*, 6950−6963.
(29) Ding, S.-Y.; Wang, W. Covalent Organic Frameworks (COFs): From Design to Applications. *Chem. Soc. Rev.* **2013**, *42*, 548−568.
(30) Babarao, R.; Jiang, J. Exceptionally High CO_2 Storage in Covalent-Organic Frameworks: Atomistic Simulation Study. *Energy Environ. Sci.* **2008**, *1*, 139−143.
(31) Sumida, K.; Rogow, D. L.; Mason, J. A.; McDonald, T. M.; Bloch, E. D.; Herm, Z. R.; Bae, T.-H.; Long, J. R. Carbon Dioxide Capture in MetalOrganic Frameworks. *Chem. Rev.* **2012**, *112*, 724−781.
(32) Canivet, J.; Fateeva, A.; Guo, Y.; Coasne, B.; Farrusseng, D. Water Adsorption in MOFs: Fundamentals and Applications. *Chem. Soc. Rev.* **2014**, *43*, 5594−5617.
(33) Qian, J.; Jiang, F.; Yuan, D.; Wu, M.; Zhang, S.; Zhang, L.; Hong, M. Highly Selective Carbon Dioxide Adsorption in a Water-Stable IndiumOrganic Framework Material. *Chem. Commun.* **2012**, *48*, 9696−9698.
(34) Wang, C.; Liu, X.; Keser Demir, N.; Chen, J. P.; Li, K. Applications of Water Stable Metal−Organic Frameworks. *Chem. Soc. Rev.* **2016**, *45*, 5107−5134.
(35) Liu, J.; Thallapally, P. K.; McGrail, B. P.; Brown, D. R.; Liu, J. Progress in Adsorption-based CO_2 Capture by MetalOrganic Frameworks. *Chem. Soc. Rev.* **2012**, *41*, 2308−2322.
(36) Ramdin, M.; de Loos, T. W.; Vlugt, T. J. State-of-the-Art of CO_2 Capture with Ionic Liquids. *Ind. Eng. Chem. Res.* **2012**, *51*, 8149−8177.
(37) Sumon, K. Z.; Henni, A. Ionic Liquids for CO_2 Capture using COSMO-RS: Effect of Structure, Properties and Molecular Interactions on Solubility and Selectivity. *Fluid Phase Equilib.* **2011**, *310*, 39−55.
(38) Gupta, K. M.; Chen, Y.; Hu, Z.; Jiang, J. MetalOrganic Framework Supported Ionic Liquid Membranes for CO_2 Capture: Anion Effects. *Phys. Chem. Chem. Phys.* **2012**, *14*, 5785−5794.
(39) Zeng, S.; Zhang, X.; Bai, L.; Zhang, X.; Wang, H.; Wang, J.; Bao, D.; Li, M.; Liu, X.; Zhang, S. Ionic-Liquid-Based CO_2 Capture Systems: Structure, Interaction and Process. *Chem. Rev.* **2017**, *117*, 9625−9673.
(40) Chen, Y.; Qiao, Z.; Lv, D.; Wu, H.; Shi, R.; Xia, Q.; Wang, H.; Zhou, J.; Li, Z. Selective Adsorption of Light Alkanes on a Highly Robust Indium Based MetalOrganic Framework. *Ind. Eng. Chem. Res.* **2017**, *56*, 4488−4495.
(41) Wu, X.; Huang, J.; Cai, W.; Jaroniec, M. Force Field for ZIF-8 Flexible Frameworks: Atomistic Simulation of Adsorption, Diffusion of Pure Gases As CH_4, H_2, CO_2 and N_2. *RSC Adv.* **2014**, *4*, 16503−16511.
(42) Mayo, S. L.; Olafson, B. D.; Goddard, W. A. DREIDING: A Generic Force Field for Molecular Simulations. *J. Phys. Chem.* **1990**, *94*, 8897−8909.
(43) Rappe, A. K.; Casewit, C. J.; Colwell, K. S.; Goddard, W. A.; Skiff, W. M. UFF, A full Periodic Table Force Field for Molecular Mechanics and Molecular Dynamics Simulations. *J. Am. Chem. Soc.* **1992**, *114*, 10024−10035.
(44) Tong, M.; Yang, Q.; Xiao, Y.; Zhong, C. Revealing the StructureProperty Relationship of Covalent Organic Frameworks for CO_2 Capture from Postcombustion Gas: A Multi-Scale Computational Study. *Phys. Chem. Chem. Phys.* **2014**, *16*, 15189−15198.
(45) Cornell, W. D.; Cieplak, P.; Bayly, C. I.; Gould, I. R.; Merz, K. M.; Ferguson, D. M.; Spellmeyer, D. C.; Fox, T.; Caldwell, J. W.; Kollman, P. A. A Second Generation Force Field for the Simulation of Proteins, Nucleic Acids, and Organic Molecules. *J. Am. Chem. Soc.* **1995**, *117*, 5179−5197.
(46) Kelkar, M. S.; Maginn, E. J. Effect of Temperature and Water Content on the Shear Viscosity of the Ionic Liquid 1-Ethyl-3-methylimidazolium Bis(trifluoromethanesulfonyl)imide As Studied by Atomistic Simulations. *J. Phys. Chem. B* **2007**, *111*, 4867−4876.
(47) Canongia Lopes, J. N.; Deschamps, J.; Pádua, A. A. H. Modeling Ionic Liquids Using a Systematic All-Atom Force Field. *J. Phys. Chem. B* **2004**, *108*, 2038−2047.
(48) Chaumont, A.; Wipff, G. Solvation of Ln(III) Lanthanide Cations in the [BMI][SCN], [$MeBu_3N$][SCN], and [$BMI]_5$Ln-$(NCS)_8$] Ionic Liquids: A Molecular Dynamics Study. *Inorg. Chem.* **2009**, *48*, 4277−4289.
(49) Plimpton, S. Fast Parallel Algorithms for Short-Range Molecular Dynamics. *J. Comput. Phys.* **1995**, *117*, 1−19.
(50) Dubbeldam, D.; Calero, S.; Ellis, D. E.; Snurr, R. Q. RASPA: Molecular Simulation Software for Adsorption and Diffusion in Flexible Nanoporous Materials. *Mol. Simul.* **2016**, *42*, 81−101.
(51) Maitland, G.; Rigby, M.; Smith, E.; Wakeham, W. *Intermolecular Forces—Their Origin and Determination*; Oxford University Press: Oxford, U.K., 1981.
(52) Potoff, J. J.; Siepmann, J. I. Vapor−Liquid Equilibria of Mixtures Containing Alkanes, Carbon Dioxide, and Nitrogen. *AIChE J.* **2001**, *47*, 1676−1682.
(53) Errington, J. R.; Panagiotopoulos, A. Z. A Fixed Point Charge Model for Water Optimized to the VaporLiquid Coexistence Properties. *J. Phys. Chem. B* **1998**, *102*, 7470−7475.
(54) Rahimi, M.; Babu, D. J.; Singh, J. K.; Yang, Y.-B.; Schneider, J. J.; Müller-Plathe, F. Double-Walled Carbon Nanotube Array for CO_2 and SO_2 Adsorption. *J. Chem. Phys.* **2015**, *143*, 124701.
(55) Crable, G. F.; Smith, W. V. The Structure and Dipole Moment of SO_2 from Microwave Spectra. *J. Chem. Phys.* **1951**, *19*, 502.
(56) Gupta, K. M.; Chen, Y.; Hu, Z.; Jiang, J. MetalOrganic Framework Supported Ionic Liquid Membranes for CO_2 Capture: Anion Effects. *Phys. Chem. Chem. Phys.* **2012**, *14*, 5785−5794.

DOI: 10.1021/acs.energyfuels.9b00179
Energy Fuels 2019, 33, 3421−3428